Origin of the 50 Hz harmonics in the transverse beam spectrum of the Large Hadron Collider

S. Kostoglou*
CERN, Geneva 1211, Switzerland and National Technical University of Athens, Athens 15780, Greece

G. Arduini, Y. Papaphilippou, and G. Sterbini
CERN, Geneva 1211, Switzerland

L. Intelisano
CERN, Geneva 1211, Switzerland and INFN, Sapienza Università di Roma, Rome 00185, Italy

(Received 8 September 2020; accepted 18 February 2021; published 8 March 2021)

Since the beginning of the Large Hadron Collider (LHC) commissioning, spectral components at harmonics of the mains frequency (50 Hz) have been observed in the transverse beam spectrum. This paper presents an overview of the most important observations, collected during the latest physics operation of the LHC in 2018, which clearly indicates that the harmonics are the result of a real beam excitation rather than an instrumental feature. Based on these findings, potential sources of the perturbation are discussed and a correlation with power supply ripple originating from the magnets' power supplies is presented.

DOI: 10.1103/PhysRevAccelBeams.24.034001

I. INTRODUCTION

In particle accelerators, studies of the beam spectrum can reveal important information concerning the existence of external noise sources that perturb the motion of the particles. Noise effects such as power supply ripple, ground motion, and the noise induced by the transverse feedback system are an important issue for the single-particle beam dynamics in past, present, and future accelerators. In the presence of nonlinearities such as nonlinear magnets and beam-beam effects, depending on the spectral components and the nature of the source, power supply ripple can act as a diffusion mechanism for the particles in the beam distribution, through the excitation of resonances in addition to the ones driven by the lattice nonlinearities, an effect that can prove detrimental to the beam lifetime [1–4]. This paper focuses on the investigation of such a mechanism that has been observed in the transverse beam spectrum of the Large Hadron Collider (LHC) [5], which is contaminated by harmonics of 50 Hz [6–9].

Observations of harmonics of the mains power frequency in the beam spectrum have been reported in the past from several accelerators including the Super Proton Synchrotron (SPS) [10–14], the Hadron-Electron Ring Accelerator (HERA) [3,15,16], the Relativistic Heavy Ion Collider (RHIC) [17,18] and the Tevatron [19,20]. The studies in the SPS excluded the factor of instrumentation noise as the origin of the perturbation and it was shown that the beam was excited by high-order harmonics, in the form of dipolar excitations, mainly affecting the horizontal plane [10]. The source of the perturbation was identified as the main dipoles by injecting an external sinusoidal ripple on their power supply.

The study conducted at RHIC demonstrated that high-order harmonics ($h > 100$) were visible in several unrelated instruments as a result of a real beam excitation rather than an artifact of the instrumentation system [17]. By modifying machine parameters such as the betatron tune and the coupling the source was identified as a dipolar field error. Through a set of experiments, a correlation with power supply ripple was established and specifically, with the 12-pulse line-commutated thyristor power supplies of the main dipoles [18].

A similar observation of 50 Hz high-order harmonics perturbing the beam spectrum in the form of dipolar excitations is also systematically made in the LHC. In this paper, we present the analysis of the experimental data acquired during the 2018 LHC operation aiming to identify the origin of the perturbation. The key observations that lead to the understanding that the harmonics are the result of a real beam excitation are presented in Sec. II. A correlation with power supply ripple arising from the power supplies of the main dipoles is confirmed with dedicated experiments for the first time in the LHC operation. The analytical formalism of dipolar power

*sofia.kostoglou@cern.ch

Published by the American Physical Society under the terms of the Creative Commons Attribution 4.0 International license. Further distribution of this work must maintain attribution to the author(s) and the published article's title, journal citation, and DOI.

supply ripple and the tracking simulations aiming to determine whether the observed power supply ripple leads to a degradation of the beam performance are treated in a second paper [21].

II. EXPERIMENTAL OBSERVATIONS IN THE LHC

Throughout this paper, the main observable is the representation of the beam signal in frequency domain as computed with the fast Fourier transform (FFT). Based on the Fourier analysis, information concerning the origin of the 50 Hz can be extracted. This can be achieved by following the evolution of the lines in frequency domain, both in terms of amplitude and phase, during normal operation, i.e., without any modification in the beam or machine parameters (Sec. II B). Then, the findings are further extended by observing the response of the harmonics during modifications in the beam or machine configuration (Sec. II C). These modifications refer to changes, first, in the betatron motion with parameters such as the tune, the phase advance and the beam energy, second, in the power supplies and last, in the settings of the transverse damper.

A. Overview of the LHC beam modes

The fact that different beam energies and phases of the LHC nominal cycle have been explored in this study justifies the need to include a brief description of the beam modes that are relevant to the next sections of this paper. Figure 1 illustrates the operational cycle for a physics fill (Fill 7333). The different beam modes (gray) are presented along with the intensity evolution of Beam 1 (blue) and 2 (red) in the right axis and the beam energy (black) in the left axis.

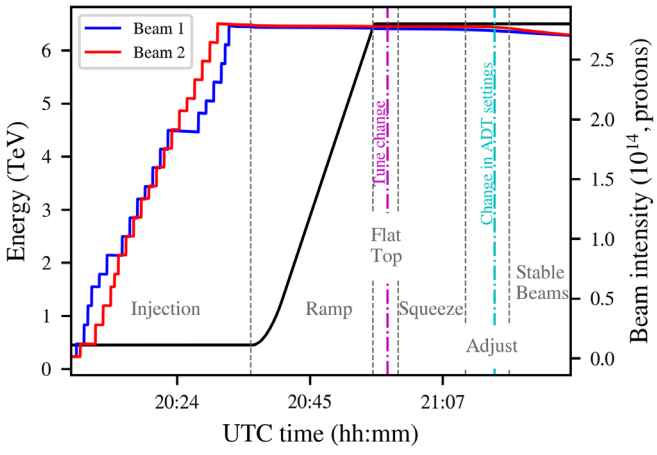

FIG. 1. The LHC operational cycle in 2018 (Fill 7333). The intensity evolution of Beam 1 (blue) and 2 (red) and the beam energy (black) are illustrated. The vertical gray lines denote the beam modes and important modifications during the cycle such as the change of tune (magenta) and the modification in the transverse damper's settings (cyan).

In brief, the nominal LHC cycle is organized as follows. After injecting low-intensity single bunches for machine protection reasons, high-intensity batches (two or three trains of 48 or 72 bunches and a bunch spacing of 25 ns) are injected from the SPS to the LHC rings until the requested filling scheme is reached. The *injection* is performed in the interaction region (IR) 2 and 8 for Beam 1 and 2, respectively, with an energy per beam equal to 450 GeV.

Then, during *ramp*, the current of the main dipoles and quadrupoles increases while the beams are accelerated. An intermediate squeeze of the β-functions at the IPs, β^*, is performed [22].

At *flat top*, each beam has reached the maximum total energy of 6.5 TeV (as compared to the nominal design total energy of 7 TeV). After a few minutes, the betatron tunes are trimmed from the injection $(Q_x, Q_y) = (0.28, 0.31)$ to the collision $(Q_x, Q_y) = (0.31, 0.32)$ values (magenta). With the achromatic telescopic squeezing (ATS) optics [23], the beams are squeezed to $\beta^* = 30$ cm at the IPs of the two high luminosity experiments (ATLAS and CMS).

During *adjust*, the separation bumps in the IRs collapse and the beams are brought to collision. At the end of this beam mode, the settings of the transverse damper are modified (cyan).

The declaration of *stable beams* signals the start of the data acquisition from the experiments. In this beam mode, luminosity optimization techniques are employed such as the crossing angle antileveling and the β^*-leveling [24,25]. Finally, the beams are extracted from the ring to the dump.

B. Beam measurements in normal operation

The concept of the 50 Hz lines on the beam spectrum is illustrated using the turn-by-turn data from the High Sensitivity Base-Band measurement system (HS BBQ) [26,27]. Figure 2 depicts the spectrogram of the horizontal plane of Beam 1 (Fill 7056) for the last few minutes of the fill, extending up to the first few minutes of the beam dump (red dashed line). The Fourier analysis for each time interval in the horizontal axis is performed with a window length of 2^{13} consecutive turns and an overlap of 2^{11} turns between windows. The frequency range is zoomed below the Beam 1 horizontal tune (≈3.49 kHz) to observe the 50 Hz harmonics in its proximity. A color code is assigned to the power spectral density (PSD) to distinguish the main spectral components (yellow and red) from the noise baseline (blue).

The spectrum clearly shows that a series of 50 Hz harmonics are present in the beam signal. The fact that the lines appear as multiples of 50 Hz and not as sidebands around the betatron tune is one of the first indications among others (see Sec. II C) that the nature of the power supply ripple is dipolar.

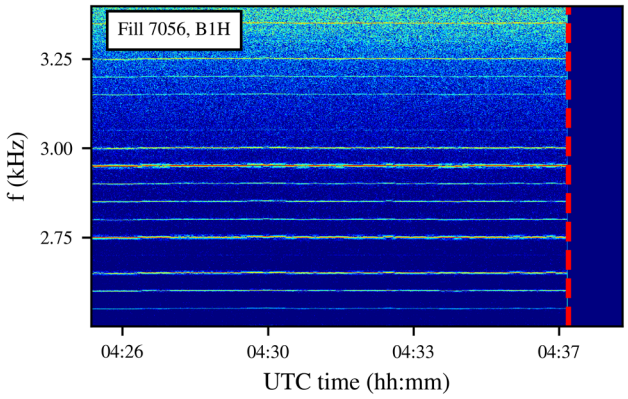

FIG. 2. Horizontal HS BBQ spectrogram of Beam 1 at the end of a physics fill (Fill 7056), centered around 3 kHz and color-coded with the PSD. The red dashed line indicates the end of the fill and the start of the dump of the beam.

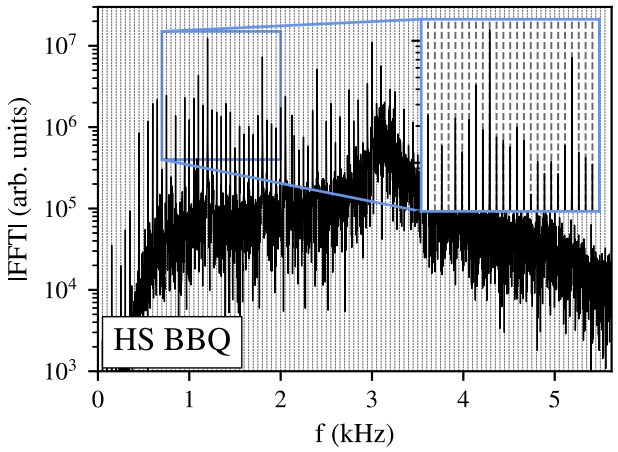

FIG. 3. The horizontal spectrum of Beam 1 at injection energy during the MD Fill 7343 from the HS BBQ and with a zoomed window (light blue). The vertical gray lines represent the multiples of 50 Hz.

Furthermore, the harmonics are visible only in the presence of the beam. All signals acquired after the end of the fill (red dashed line) are dominated by the noise of the instrument. A comparison between the signals prior and after the dump of the beam provides a first indication that the lines do not emerge as a by-product of instrumentation noise.

To further exclude the factor of instrumental or environmental noise, the presence of these harmonics has been validated from several unrelated beam instruments. Position measurements from multiple pickups, located at different positions in the LHC ring, are collected. The main observables are the HS BBQ, the transverse damper observation box (ADTObsBox) [28–30], the diode orbit and oscillation system (DOROS) [31,32] and the multiband instability monitor (MIM) [33,34]. Measurements from all the aforementioned instruments are available for the machine development (MD) Fill 7343, dedicated to studies concerning the 50 Hz harmonics [35].

Figure 3 shows the spectra for one of these instruments, the HS BBQ, for the horizontal plane of Beam 1, while the vertical gray lines represent the multiples of 50 Hz. To illustrate that the lines in the beam spectrum correspond to 50 Hz harmonics, a zoomed region of the spectrum is depicted (light blue). From the analysis of the various spectra, it is confirmed that a series of 50 Hz harmonics is visible across all unrelated instruments.

The turn-by-turn acquisitions, such as the ones from the HS BBQ and DOROS, allow accessing a frequency regime up to approximately 5.6 kHz, which is the Nyquist frequency assuming a single observation point along the accelerator (the sampling frequency is $f_s = f_{\mathrm{rev}}$ with $f_{\mathrm{rev}} = 11.245$ kHz) [36]. If present in the signal, frequency components beyond this limit will be aliased in the spectrum.

On the contrary, the ADTObsBox and the MIM provide high sampling rate measurements. Specifically, the ADTObsBox instability buffer contains calibrated bunch-by-bunch position measurements for 2^{16} turns. Firstly, the fact that a calibrated metric is provided allows computing the offsets induced on the beam motion from the 50 Hz harmonics. Secondly, the bunch-by-bunch information is needed to study the evolution of the 50 Hz in the cycle and to compute a high bandwidth spectrum, in the presence of a regular filling scheme.

As shown in the Appendix A, the noise floor of the single-bunch ADTObsBox spectrum exceeds the amplitude of the 50 Hz harmonics and therefore, a decrease of the noise baseline is necessary to study their evolution during the cycle. To overcome this problem, a method to combine the information from several bunches has been developed, taking into account the dephasing of the spectrum, due to the time delay, across the different bunches (Appendix A). Assuming a regular filling scheme (equal spacing between bunches), this signal averaging algorithm not only provides a reduction of the noise floor but also extends the measurable frequency range of the beam spectrum, while suppressing the aliases and preserving the signal metric.

The horizontal spectrum of Beam 2 is computed for the physics Fill 7334 during collisions, using the bunch-by-bunch and turn-by-turn acquisitions from the Q7 pickup of the ADTObsBox. Although only the spectrum of Beam 2 is depicted, similar observations exist for both beams and planes.

Figure 4 illustrates the Fourier analysis, first, for a frequency range up to 10 kHz (Fig. 4 top). From the review of the spectrum, two areas of particular interest are identified. The first regime (blue span) consists of 50 Hz harmonics extending up to 3.6 kHz. The second area (orange span) is a cluster of 50 Hz at 7–8 kHz. In particular, the cluster is centered at the frequency $f_{\mathrm{rev}} - f_x$, where f_x is the horizontal betatron frequency, which is ≈3.15 kHz at

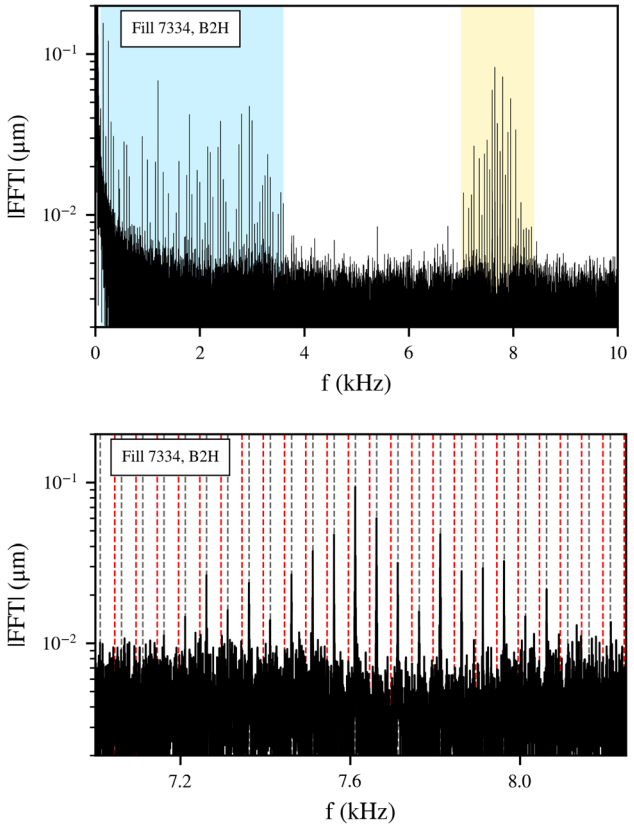

FIG. 4. The horizontal spectrum of Beam 2 at Flat Top for a frequency range up to 10 kHz (top), with the low and high-frequency cluster indicated by the blue and orange span, respectively, and centered around the high-frequency cluster (bottom). The red and gray dashed lines represent the expected position of aliased ($f_{\mathrm{rev}} - f_{50}$) and physical 50 Hz harmonics (f_{50}), respectively.

injection and ≈3.49 kHz at collision energy(see also Sec. II C). In the frequency interval between the two clusters, either no harmonics are present in the signal or their amplitude is below the noise threshold of the instrument.

Throughout this paper, the two regimes of interest are referred to as the *low-frequency cluster* and the *high-frequency cluster*, respectively. It must be noted that the lowest order harmonics are excluded from the analysis as their amplitude is affected by the noise of the instrument. Then, the calibrated spectrum indicates that the harmonics of the high-frequency cluster are more important in terms of amplitude.

As the high-frequency cluster is situated at $f_{\mathrm{rev}} - f_x$, the question that naturally arises is whether these frequency components emerge from aliasing. In fact, even in the case of a physics fill, the sampling rate is only approximately uniform as not all trains are equally spaced. This error can give rise to the aliasing of the low-frequency cluster around the revolution frequency. It must be noted however, that the beam revolution frequency ($f_{\mathrm{rev}} = 11.245$ kHz) is not a multiple of 50 Hz and therefore, the aliases can be distinguished from the excitations at 50 Hz.

Figure 4 (bottom) presents the spectrum centered around the high-frequency cluster. The red dashed lines represent the expected position of aliased 50 Hz harmonics $f_{\mathrm{rev}} - f_{50}$, where f_{50} are the harmonics of the low-frequency cluster, while the gray dashed lines illustrate the multiples of 50 Hz $f_{50} = h \cdot 50$ Hz, where h is a positive integer. As the spectral components of the high-frequency cluster coincide with the 50 Hz multiples (gray), it is concluded that they are not aliased frequencies.

The time variation of the beam spectrum can reveal important information concerning the source of the perturbation. Due to the variation of the power grid load, the frequency of the mains power supply is not strictly 50 Hz. The study focuses on the impact of the aforementioned drift on the frequency evolution of the 50 Hz harmonics in order to illustrate their distinct signature in the frequency domain.

The spectrogram of the horizontal position of Beam 1 is computed from the MIM data for a time interval at stable beams. In Fig. 5, the horizontal axis represents the time-stamp of each spectrum with a window length of 2^{14} turns, the vertical axis is centered around a value in the low (left) and high (right) frequency cluster and a color code is assigned to the PSD.

An important finding is that, although the lines are harmonics of 50 Hz, a time variation of their frequency is observed. Specifically, all harmonics evolve in a similar manner, but the size of the frequency shift is proportional to the order of the harmonic h as shown in Fig. 5. For this reason, the aforementioned effect is more pronounced in the harmonics of the high-frequency cluster, an observation which provides yet another indication that these components are not aliases.

To illustrate quantitatively that the harmonics experience a similar frequency evolution, the amplitude of which scales with the order of the harmonic h, an algorithm that can precisely follow their evolution has been implemented. The steps of the algorithm are the following: for each

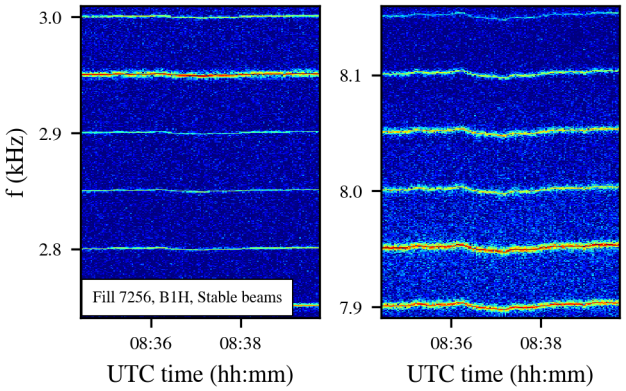

FIG. 5. The horizontal spectrogram of Beam 1 in a regime of the low (left) and high (right) frequency cluster.

measured time interval the amplitude of the Fourier spectrum is computed. The algorithm focuses on a regime in the vicinity of a single harmonic and, by employing a maximization routine, an accurate determination of its frequency is achieved by detecting the local maximum. The algorithm returns the frequency and the amplitude of the harmonic at each time step. This procedure is repeated for all the time intervals in the spectrogram.

Iterating over all the harmonics in the spectrum with the aforementioned algorithm validates the existence of a similar frequency evolution with an amplitude proportional to the order of the harmonic. Figure 6 shows the frequency evolution of all the harmonics (black) after normalizing with the order of the harmonic h and projecting to the fundamental frequency (50 Hz). This evolution is visible in both beams and planes, during all beams modes and across several unrelated instruments. An explanation on the proportional relationship between the amplitude and the harmonic order is presented in Appendix B.

Figure 6 also presents the evolution of the network frequency for the same time span (green) [37]. The origin of the similar frequency evolution in the harmonics of the beam is clearly related to the stability of the 50 Hz mains from the electrical network, which then propagates to all the harmonics.

The beam spectrum is compared to the output voltage spectrum of the main bends power supply installed in sector 1-2. During the MD Fill 7343, voltage measurements of the power supply were collected every minute with a sampling rate of 50 kHz. The supply's voltage spectrum consists of 50 Hz harmonics, extending up to 10 kHz. Applying a similar analysis to the one used for the harmonics of the beam yields an identical frequency evolution of the 50 Hz components in the power supply. Figure 6 presents the evolution of the lines in the power supply down-sampled to 50 Hz (blue).

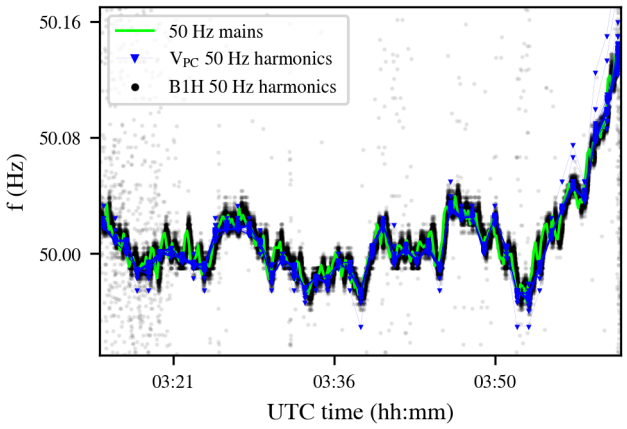

FIG. 6. The mains power supply ripple frequency (green), the frequency evolution of the harmonics observed in the voltage spectrum of the main dipoles power supply of sector 1-2 (blue) and the ones of the beam spectrum (black), after normalizing with the order of each harmonic h.

It is interesting to note that, at the end of the MD (6 am Central European Time or 4 am in Coordinated Universal Time), a frequency drift above the usual variation of the 50 Hz is observed. To validate that this effect is reproducible, fills for the same time and different days have been analyzed, yielding similar results. These variations appear to be the result of the changing load of the power grid at this time of the day.

The previous findings are not meant to establish a correlation between the dipole power supply in sector 1-2 and the beam. The importance of these observations resides on the fact that, if the 50 Hz harmonics are the results of a real beam excitation, their frequency domain signature points to a specific type of power supply as the source.

The existence of multiple 50 Hz harmonics in combination with the similar frequency evolution induced by the mains suggests that the origin of these frequency lines are power supplies that are based on commutated Thyristor Technology. This can be understood with a frequency analysis of the variation of the magnetic field (B-Train) in two other machines of the accelerator complex: the Proton Synchrotron (PS) and the and SPS [38,39]. In the B-Train system, a pickup up coil is installed in the aperture of the reference dipole magnets. The measured signals correspond to the rate of change of the magnetic field.

Figure 7 shows the spectrogram of the magnetic measurements for the PS (top) and SPS (bottom). The PS spectrum reveals a strong component at 5 kHz, which is the frequency of some of its Switch-Mode power supplies [40]. The switching of this type of power supply is regulated by a clock. Subsequently, a negligible variation in the frequency evolution of the line is observed. As the switching frequencies are well defined, they can be easily identified and no 50 Hz harmonics are present in the signal.

On the contrary, in the SPS case, the power supply is a silicon controlled rectifier (SCR). Hence, the 50 Hz harmonics are visible on the signal and the stability of the mains has an impact on the output current of the power supplies. In the following studies, when the expected position of the 50 Hz harmonics is illustrated, the drift of the harmonics due to this evolution is taken into account. The presence of 50 Hz harmonics in the output of a SCR power supply is explained with a simplified model in Appendix C.

Therefore, if environmental noise is excluded as the origin of the perturbation, the signature of the 50 Hz harmonics in the beam spectrum suggests that the possible sources are limited to magnets with SCR power supplies. The magnets powered by SCR in the LHC are presented in Table I [41,42].

The phase evolution of the 50 Hz harmonics between two locations in the ring can clarify whether the power supply ripple lines are the result of a real beam excitation. To this end, their phase advance is measured between two

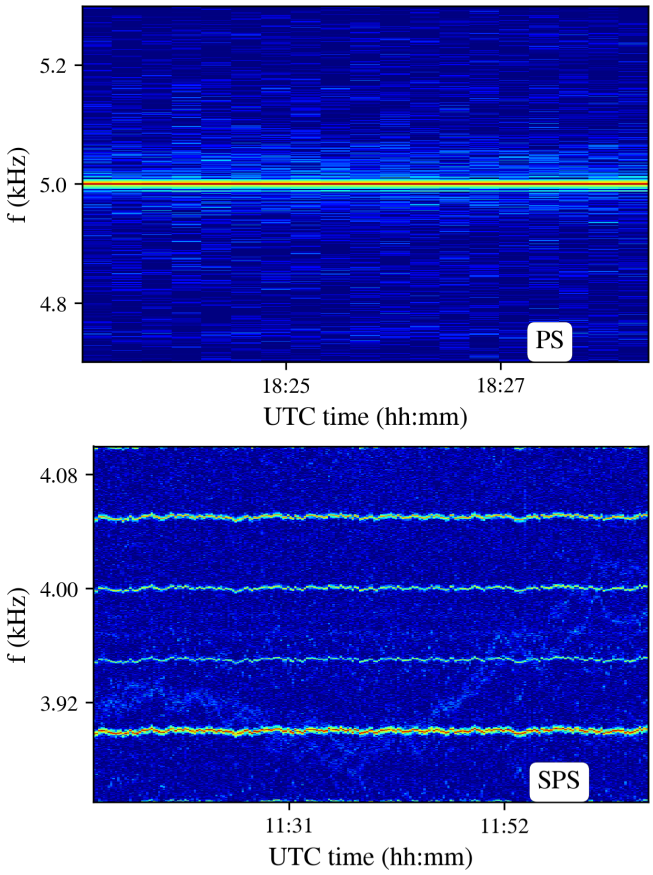

FIG. 7. The spectrum of the B-Train in PS (top) and SPS (bottom). The strong component at 5 kHz in the PS spectrum is one of the switching frequencies of the switch-mode power supply. The SPS spectrum illustrates the signature of a SCR power supply, which is characterized by a series of 50 Hz harmonics with a similar frequency evolution induced by the mains.

closely separated pickups and compared to the betatron phase advance between the same pickups. For the validity of the comparison, the two observation points must be situated in a relatively close distance, so that the beam does not encounter a noise perturbation while crossing this path.

TABLE I. The SCR power supplies in the LHC [41,42].

Power supply type	Use
RPTE	Main dipoles
RPTF	Warm quadrupoles (Q4, Q5)
RPTG	Dogleg dipoles (D1-D4, spare)
RPTL	Alice compensator
RPTM	Dump septa
RPTI	Alice and LHCb dipoles
RPTN	LHCb compensator
RPTJ	CMS Solenoid
RPTH	Alice Solenoid
RPTK	RF Klystron

If the harmonics are a by-product of noise in the beam instrumentation then their phase advance is not expected to correspond to the betatronic one. Furthermore, an arbitrary dephasing between the low and high-frequency cluster should be observed. On the contrary, in the case of a real excitation, the power supply ripple phase advance must correspond to the betatronic one for all the harmonics present in the spectrum.

Two pickups of the transverse damper, referred to as Q7 and Q9, are selected for the analysis. At collision energy, the betatron phase advance between the two observation points is defined by the optics and it is approximately equal to 110 degrees. The first step is to compute the complex Fourier spectra for a single pickup and for each bunch in a physics fill to observe the dephasing of the lines across the full machine. As previously reported, with the present noise floor, the evolution of the lines cannot be determined with a single bunch. For this reason, the average signal is computed from five consecutive LHC trains, each one of which consists of 48 bunches. Then, the phase evolution of each harmonic is computed across the accelerator.

Figure 8 depicts the dephasing of a harmonic in the high-frequency cluster ($h = 156$) as a function of the train number for Q7 (blue) and Q9 (green). The cyan lines illustrate the expected dephasing, which is proportional to the frequency and the time delay of the trailing trains from the first train in the machine (Appendix A). It must be noted that by averaging over a few consecutive trains the signal is subsampled to f_{rev}, similarly to the single bunch case. The negative slope of the 7.8 kHz line shows that the phase evolution of the harmonic was computed through aliasing, i.e., by following the phase evolution of the reflected frequency component around the revolution frequency ($f_{\mathrm{rev}} - 7.8$ kHz). The phase advance of each harmonic is the difference in the phase determination of the two pickups. A correspondence to the betatron phase advance is found, an observation that clearly proves, for the first

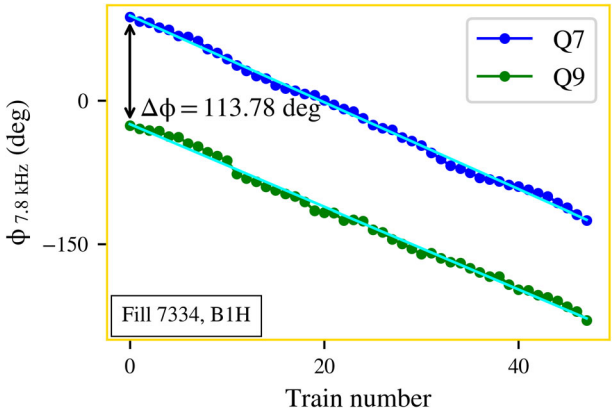

FIG. 8. The phase evolution of the $h = 156$ harmonic as a function of the train number for Q7 (blue) and Q9 (green). The cyan lines illustrate the expected phase evolution of the harmonics in the accelerator (Appendix A).

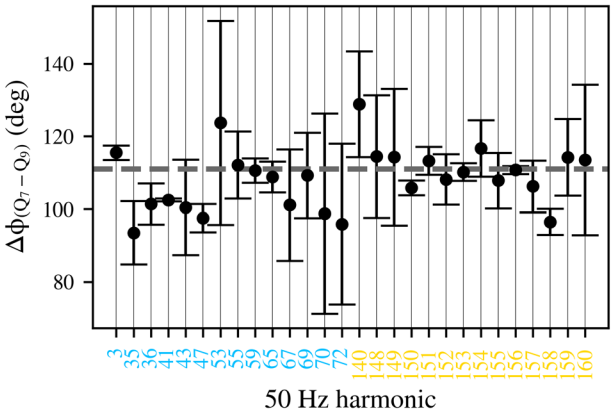

FIG. 9. The average phase advance from Q7 to Q9 for the harmonics in the low (blue) and high (orange) frequency cluster. The error bars represent one standard deviation and the gray dashed line illustrates the betatron phase advance (110 degrees).

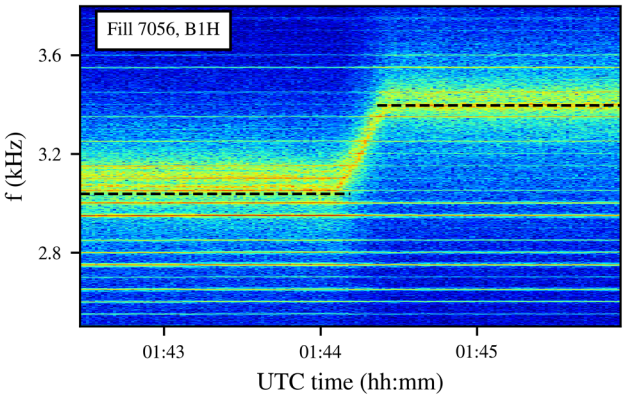

FIG. 10. The horizontal spectrogram of Beam 1 at flat top. The black dashed lines represent an approximation of the injection and the collision tune in the horizontal plane.

time, that the two harmonics correspond to a real beam excitation. Similar results are obtained for all the harmonics present in the beam spectrum.

The filling scheme of the physics Fill 7334 is divided in three groups of consecutive trains. Each group corresponds to approximately one-third of the total beam. The average value and the standard deviation of the dephasing between Q7 and Q9 are computed from the three groups for all the harmonics above noise level.

Figure 9 demonstrates the average phase advance for the harmonics in the low (blue) and high (orange) frequency cluster. The error bars represent one standard deviation since following the frequency drift of lower-amplitude harmonics can introduce uncertainties. The gray dashed line indicates the betatron phase advance. The average value demonstrates that, within an uncertainty represented by the standard deviation, the phase advance for all the harmonics is the one of the beam, thus proving that the observations are not instrumental.

C. Observations during changes in the beam and machine configuration

The response of the harmonics during a simple modification of the betatron motion such as the change of the tune at flat top is investigated. Figure 10 presents the HS BBQ spectrogram for the horizontal plane of Beam 1 in the physics Fill 7056. The spectrogram is centered around the betatron tune for the whole duration of flat top and a color code is assigned to the PSD. The black dashed line represents an approximation of the horizontal tune evolution.

First, one must observe that the frequencies of the lines are not affected by the tune change. This fact proves that the harmonics are the result of a dipolar field error rather than a tune modulation [43]. Second, a comparison prior and after the trim leads to the conclusion that the amplitude of the lines in the vicinity of the betatron tune is strongly enhanced. This resonant behavior is in agreement with a dipolar perturbation, with an excitation frequency that approaches the betatron tune [21].

To investigate the impact of the tune change on the high-frequency cluster, the high bandwidth spectrum is computed from the ADTObsBox prior and after the tune trim. Figure 11 shows the horizontal spectrum of Beam 2 up to 10 kHz (top) at flat top with the injection (blue) and collision (black) tune. Similar observations exist for both beams and planes.

The closest harmonics to the tune of the low-frequency cluster are enhanced in terms of amplitude. A shift is also observed at the position of the high-frequency cluster. To further illustrate this effect, the spectrum is centered around the high-frequency cluster in Fig. 11 (bottom). Although the effect is dipolar in both cases (the harmonics coincide with the 50 Hz multiples indicated with the gray lines), this observation shows that the location of the cluster is at $f_{\mathrm{rev}} - f_x$ and thus, depends on the betatron tune. The fact that the changes in the beam configuration affect the amplitude of the power supply ripple lines provides further proof that the harmonics are the result of a real beam excitation.

The response of the harmonics is studied when another modification is applied to the betatron motion and specifically, to its phase advance, while the tune is constant. During the MD Fill 6984, the betatron phase advance between the interaction point (IP) 1 and 5 were modified [44]. This was achieved through the incorporation of a set of optics knobs, which allow scanning the phase between the two IPs, based on the ATS scheme [23]. The knobs lead to a trim in the current of the quadrupole families responsible for the control of the tune. Throughout these modifications, the betatron tune is constant.

Figure 12 illustrates the supply current for a single quadrupole (red). The evolution of the current corresponds to a change of the phase advance within a range of

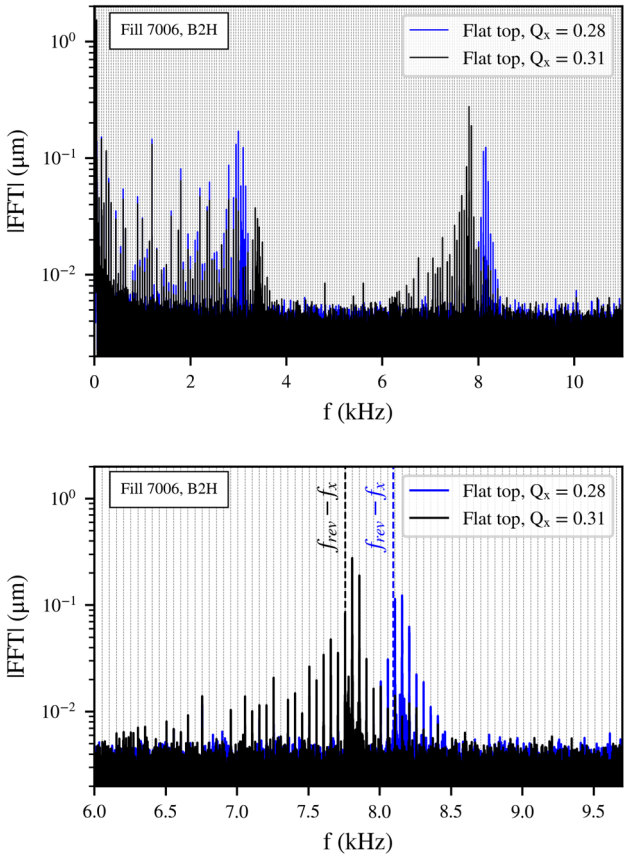

FIG. 11. The horizontal spectrum of Beam 2 prior (blue) and after (black) the tune change at flat top in a frequency range up to 10 kHz (top) and centered around the high-frequency cluster (bottom). The gray dashed lines represent the multiples of 50 Hz. The dashed blue and black vertical lines illustrate the location of $f_{\mathrm{rev}} - f_x$.

± 20 degrees for the horizontal plane of Beam 1. During this time interval, the amplitude evolution of the harmonics is computed.

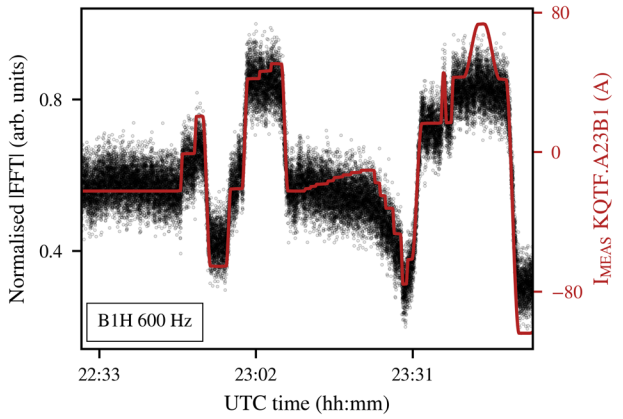

FIG. 12. The amplitude evolution of the 600 Hz lines (black) during the change of the phase advance between IP1 and IP5. while the tune is kept constant. The red line represents the current in the quadrupole trims employed for the phase scan.

Figure 12 also denotes the response of the $h = 12$ harmonic (black curve). The amplitude evolution of the lines in the low-frequency cluster is clearly impacted by the variation of the betatron phase advance, an effect that provides definitive indications that they correspond to actual beam motion. As far as the high-frequency cluster is concerned, no impact is observed in their amplitude evolution throughout these tests, which is possibly due to the mitigation of these lines from the transverse damper as shown later in this paper.

Following the change of the betatron tune and phase advance, we explore the evolution of the spectrum across different beams modes and thereby, different energies and optics. Some of the magnets in Table I can be excluded as potential sources by observing the evolution of the spectrum across the cycle.

First, due to the fact that the 50 Hz harmonics are systematically present in all beam modes and fills, the power supplies of the spare magnets and the septa are excluded. Specifically, the separation/recombination dipoles D1-D4 are currently powered by switch-mode power supplies, while the SCR power supplies of these dipoles are only used in case of failure. An analysis of the fills where the spare SCR power supplies were employed did not reveal any modification on the beam spectrum and thus, can be excluded. In addition, the magnetic field of the dump septa only affects the beam during extraction and not in operation.

Second, the amplitude of the power supply ripple lines does not significantly attenuate with increasing beam energy. Considering a non-ramping power supply as the source, a reduction of the angular deflection and thus, of the amplitude of the power supply ripple, should be observed with increasing beam rigidity. The absence of such an attenuation leads to the conclusion that the power supply ripple originates from a ramping power supply. Consequently, all non-ramping power supplies can also be excluded.

Through this process of elimination, the remaining candidates of Table I are the main dipoles and the warm quadrupoles. Combining this finding with previous indications of the dipolar nature of the source, the investigation focuses on the power supplies of the main bends. The main dipoles have undoubtedly the highest filling coefficient in the ring and, as previously mentioned, the studies conducted in other synchrotrons have proved that the arc circuit was systematically the dominant contributor.

Based on the previous findings, the pursued investigations focus on the main dipoles circuit. To establish a correlation between the harmonics of the beam and the ones in the output of their power supplies, a modification in the configuration of the latter is needed. An important observation was made when the status of the active filters of the Main Bends, which are installed for the attenuation of the

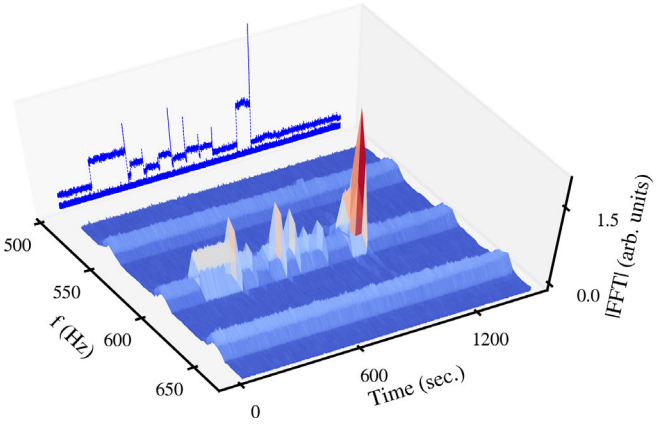

FIG. 13. The horizontal spectrogram of Beam 1 during the tests of the active filters at injection centered around 600 Hz. The blue lines represent the amplitude evolution of the spectral components in this regime.

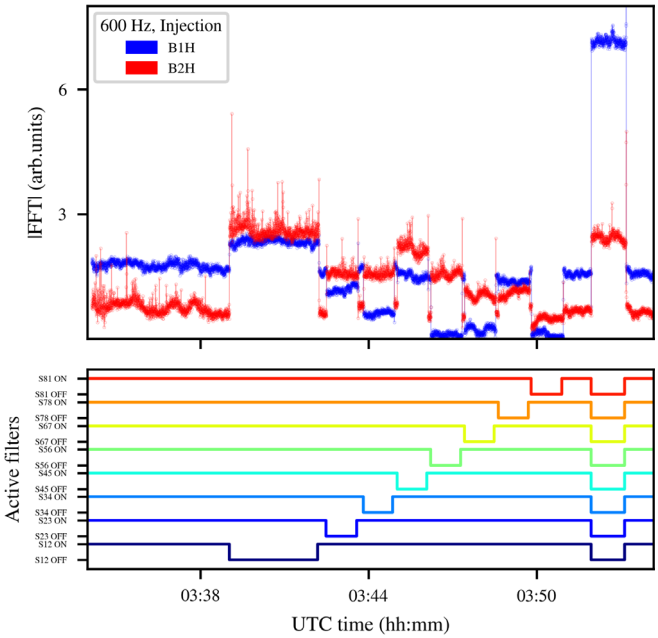

FIG. 14. The response of the $h = 12$ harmonic (top) during the tests with the active filters for Beam 1 (blue) and Beam 2 (red) at injection energy. The status of the active filters is color-coded with the sector number (bottom).

50 Hz ripple [45–47], was changed. During dedicated MD fills, the eight active filters were disabled sector-by-sector.

Figure 13 depicts the 3D spectrogram for the horizontal plane of Beam 1, as acquired from the MIM, for the time interval of the tests conducted at injection (Fill 7343). For a first demonstration, the frequency range is limited around 600 Hz. The projection of the spectrogram, which represents the amplitude evolution of the $h = 12$ harmonic, is shown with the blue curve. Disabling the eight filters leads to abrupt changes in its amplitude evolution.

The amplitude evolution of the $h = 12$ harmonic is extracted from the 3D spectrogram. Figure 14 (top) presents the response of the 600 Hz line in Beam 1 (blue) and 2 (red) at injection energy. The status of the eight active filters is presented for the same time span (bottom) and a color code is assigned to each sector. The distinct changes in the amplitude coincide with the disabling of the filter of each sector. As a last step, the filters were disabled simultaneously, which led to an important increase in the amplitude of the line. Similar observations are collected by conducting the same tests at top energy.

The observations on the $h = 12$ harmonic provide evidence that all eight power supplies contribute to this effect. The question that arises is whether the most impacted sectors in terms of power supply ripple can be identified. Reviewing the results of Fig. 14 yields that the positive or negative impact of the filter compared to the baseline, which is defined as the amplitude of the harmonic prior to the test, depends on the sector. For instance, at injection in Beam 1, disabling the Filter of sector 1-2 leads to an increase of the ripple amplitude. Therefore, the filter, when active, suppresses the harmonic and its impact is characterized as positive. On the contrary, sector 5-6 has a negative contribution at injection. Then, comparing the same sector across the two beams reveals a different impact between the two (e.g., sector 5-6 at injection). This can be possibly attributed to the different phase advance of the two beams in the ring. Finally, a comparison between the results at injection and top energy reveal that the contribution for the same beam and sector also depends on the beam energy.

The correlation with the power supplies is not only valid for the 600 Hz line, but for most of the 50 Hz harmonics included in the low-frequency cluster. Figure 15 shows the amplitude evolution of various harmonics at injection, represented with a different color code. The abrupt changes in the amplitude when disabling the active filter of each sector are reproduced for harmonics up to 3.6 kHz. In addition to the observations at 600 Hz, the contribution of each sector also varies across the harmonics.

Applying a simple modification in the configuration of the dipole power supplies, such as modifying the status of the active filters, has a direct impact on the low-frequency cluster harmonics of the beam. These results provide evidence that the power supplies of the main dipoles are the source of the harmonics up to 3.6 kHz observed in the beam spectrum. It is the first time that such a correlation has been demonstrated in the LHC. As no modifications are envisaged for the power supplies of the main dipoles, this perturbation is expected to be present also in the future upgrade of the LHC, the High Luminosity-LHC (HL-LHC) [48]. It must also be underlined that no change in the amplitude evolution of the harmonics in the high-frequency cluster is reported during these tests.

Figure 16 demonstrates the voltage spectrum of the power supply in one of the LHC sectors, first, when the active filter is enabled (top) and, then, disabled (bottom).

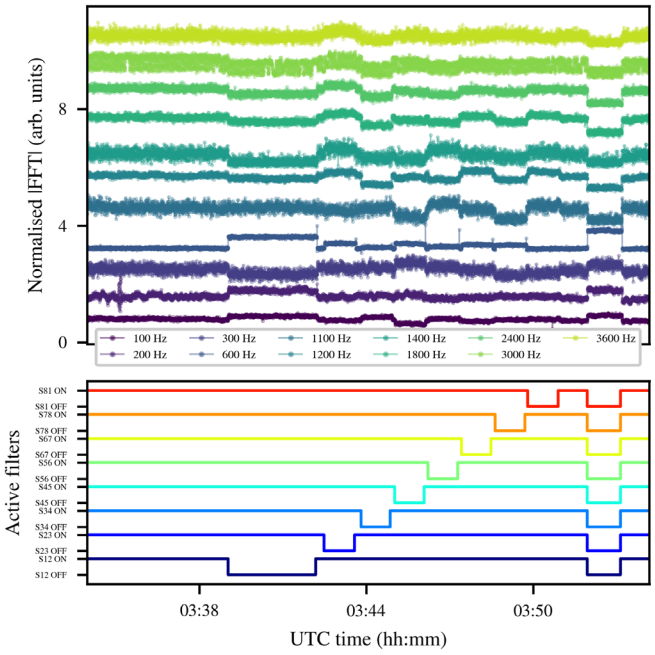

FIG. 15. The amplitude evolution of the harmonics in the low-frequency cluster (up to 3.6 kHz) during the tests with the active filters. The status of the active filters is color-coded with the sector number (bottom).

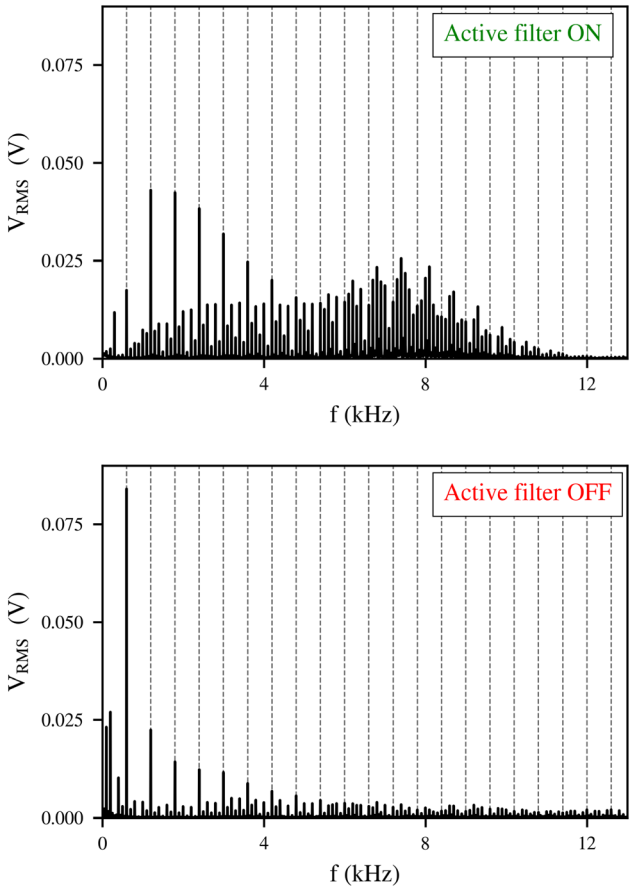

FIG. 16. Voltage spectrum of the power supply of the main dipoles in one of the LHC arcs (Sector 1-2) with the active filter enabled (top) and disabled (bottom). The vertical gray lines represent the multiples of 600 Hz.

In this case, the vertical lines represent the multiples of 600 Hz. The comparison of the spectrum prior and after the modification shows that the active filter is suppressing some of the harmonics up to approximately 3 kHz, while it enhances the high-order harmonics [47]. However, the amplitude of the high-frequency cluster in the beam spectrum did not increase when disabling the active filter possibly due to the interplay of this cluster with the transverse damper as explained later in the present paper.

The spectra of both beams and planes in a physics fill are measured and compared. As the pickups for the two beams and planes are located at different positions in the ring, the ADTObsBox calibrated spectra are normalized with the corresponding β-functions. The β-functions at the location of the ADTObsBox Q7 pickup for both beams and planes, at injection and top energy are listed in Table II.

Figure 17 shows the spectra for the horizontal (magenta) and vertical (cyan) plane for Beam 1 (left) and 2 (right). Comparing the amplitudes of the spectral lines yields that the perturbation is mainly affecting the horizontal plane, an effect compatible with a field error of the main dipoles. Due to the transverse coupling of the machine, an attenuated perturbation is also present in the vertical plane. To demonstrate that this effect results from the coupling, controlled excitations have been applied using the transverse damper during dedicated experiments. Although only the horizontal plane was excited, the oscillation was visible also in the vertical plane. To further validate the hypothesis that the 50 Hz harmonics in the vertical plane originate from coupling, a variation of the coupling will be performed in the future operation of the accelerator, while observing the impact on the harmonics' amplitude.

The maximum offset observed in the horizontal spectrum of Beam 1 is approximately 0.1 μm, which corresponds to 10^{-3} σ. As shown in [21], assuming a single dipolar perturbation, this value corresponds to a deflection of 0.09 nrad at a location with $\beta = 105$ m for an excitation frequency in the vicinity of the tune ($|Q - Q_p| = 5 \times 10^{-3}$, where Q is the betatron tune and Q_p is the ripple tune). Comparing the equivalent kick with the bending angle of a

TABLE II. The β-functions at the position of the Q7 pickup per beam and plane with injection and collision optics ($\beta^* = 30$ cm).

Beam	Plane	β at injection (m)	β at collision (m)
1	Horizontal	130.9	100.7
1	Vertical	173.6	99.6
2	Horizontal	151.1	109.6
2	Vertical	166.3	166.3

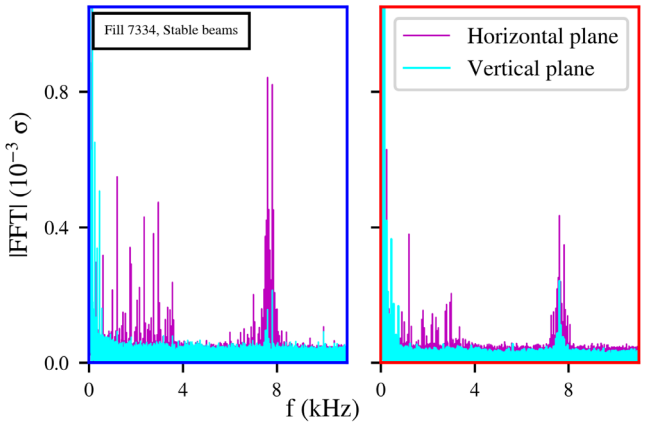

FIG. 17. The spectrum of the horizontal (magenta) and vertical (cyan) plane of Beam 1 (left) and 2 (right) in stable beams, normalized with the corresponding β-functions.

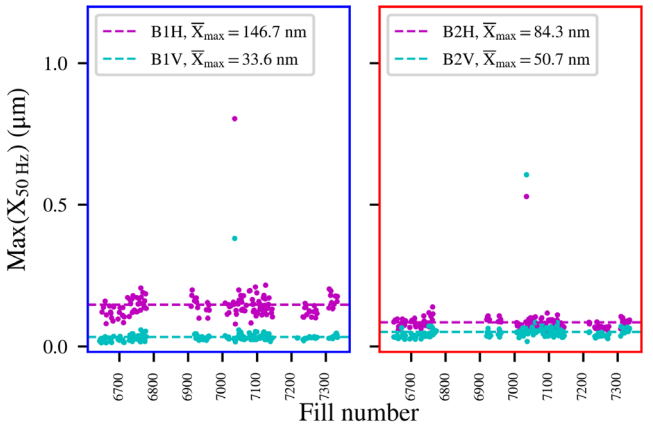

FIG. 18. The maximum amplitude of the 50 Hz harmonics for the horizontal (magenta) and vertical plane (cyan) of Beam 1 (blue) and 2 (red) for all the proton physics fills of 2018.

single dipole in the LHC (≈5 mrad) and neglecting additional effects (e.g., transverse damper, magnet's beam screen) yields a field stability of 1.8×10^{-8}, a value which is well within the power supply specifications.

Comparing the spectra of the two beams yields an asymmetry in the amplitude of the ripple between Beam 1 and 2 and that a more significant effect is visible in Beam 1. To verify the reproducibility of this observation, the spectra of both beams and planes are computed for all the proton physics fills of 2018. For each fill, the maximum offset induced by the 50 Hz harmonics is computed, which corresponds, in stable beams, to a frequency of 7.7 kHz.

Figure 18 depicts the maximum amplitude observed in the spectrum as a function of the fill number for the horizontal (magenta) and vertical (cyan) plane in Beam 1 (blue) and 2 (red). The dashed lines represent the average offset over all the fills for each plane. These results confirm that the power supply ripple is systematically more pronounced in Beam 1 than Beam 2 by approximately a factor of two in the horizontal plane. Although the dipole power supplies are common for both beams, this discrepancy is possibly attributed to the different phase advances of the two beams in the accelerator.

The fill-by-fill analysis of the spectra in Fig. 18 reveals an increase of the ripple amplitude in the physics Fill 7035. An additional parameter that has not been included in the analysis so far is the activity of the transverse damper and the interplay with the 50 Hz harmonics.

In the nominal LHC cycle, the ADT settings are modified and in particular, the extended ADT bandwidth is changed to standard bandwidth at the end of adjust [49,50]. An increase in the gain of the transverse damper is reported for the standard bandwidth compared to the extended one. In the Fill 7035, this modification was not applied and the extended bandwidth was used at stable beams.

Figure 19 illustrates the horizontal spectrum of Beam 2 at stable beams centered around the low (left) and high (right) frequency cluster and for the Fills 7033 (top) and 7035 (bottom) with the standard ADT bandwidth and extended bandwidth, respectively. Comparing the two spectra yields an increase in the amplitude of the 50 Hz

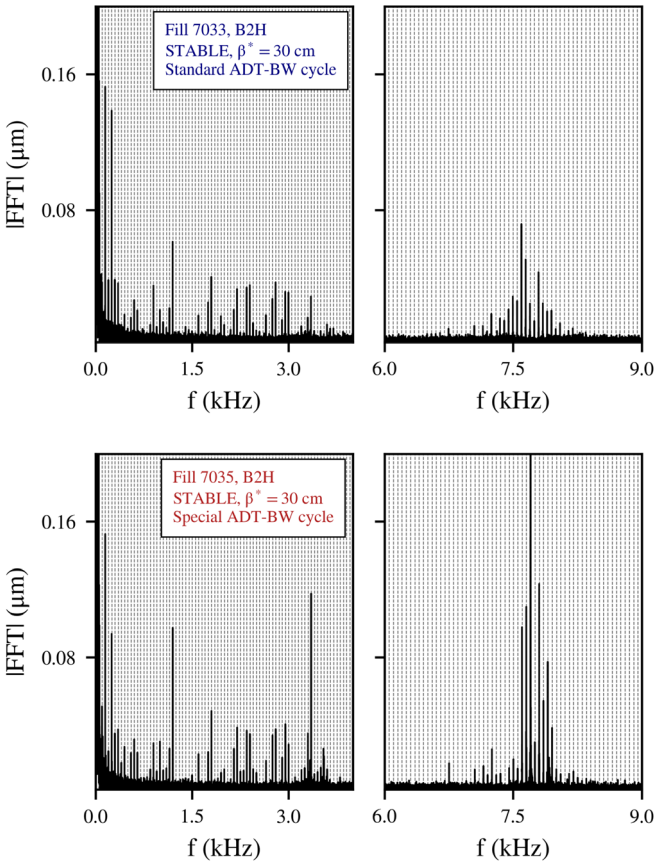

FIG. 19. The horizontal spectrum of Beam 2 at stable beams centered around the low (left) and high (right) frequency cluster for a fill with the standard (Fill 7033, top) and (b) extended (Fill 7035, bottom) ADT bandwidth.

harmonics in the regime above 3 kHz, which is particularly important for the high-frequency cluster.

This observation indicates that the amplitudes of the high-order harmonics are reduced by the damper in normal operation. This also explains why an amplitude increase of the high-frequency cluster was not observed when the corresponding harmonics in the power supply's voltage spectrum increased during the active filters tests. The impact of the ADT settings is also systematically observed in other beam modes of the machine cycle during which the bandwidth was modified such as the adjust.

The importance of this finding resides on the fact that a strong asymmetry is present between the frequencies of the low and high cluster in terms of amplitude. In particular, these observations indicate that, lowering the transverse damper gain or in the absence of the damper, the amplitude of the harmonics in the high-frequency cluster is expected to be further enhanced compared to the values that have been observed experimentally.

In contrast, Fig. 16 shows that the ripple in the power supply voltage spectrum attenuates with increasing frequency. Although the active filters enhance the high-order harmonics in the power supply voltage spectrum, their amplitude is still lower than the ones of the low-order harmonics. Furthermore, high-frequency perturbations such as the high-frequency cluster strongly exceed the cutoff frequency of the LHC main dipoles due to the shielding effect of the beam screen [51]. To this end, if the high-frequency cluster is driven by a direct excitation due to power supply ripple, a significant attenuation of its amplitude should be observed compared to the low-frequency cluster, while experimentally we observed the opposite.

Additionally, it should be mentioned that the increase of the power supply ripple by a factor of two in Fill 7035 did not lead to an increase of losses or emittance growth compared to the rest of the fills. However, as the duration of the fill was limited to 40 minutes, the impact of the power supply ripple lines on the beam lifetime cannot be excluded.

To conclude, Table III presents a summary of the most important experimental observations for each cluster. Combining this information suggests that, rather than a direct excitation, the high-frequency cluster is the result of the interplay between ripple in the dipole power supplies and a mechanism originating from the beam. The transfer function from the power supply voltage to the magnetic field seen by the beam does not consider the beam's response. Therefore, the asymmetry between the two clusters can be explained if there is a higher sensitivity of the beam's response in the regime $f_{\mathrm{rev}} - f_x$ compared to f_x, leading to important offsets from small power supply ripple perturbations at these frequencies. A potential candidate is the interplay of the beam with the machine transverse impedance, as the first unstable mode is at $f_{\mathrm{rev}} - f_x$ [52]. Other ripple sources such as the uninterruptible power supply (UPS) system must be investigated [53] during the next operation of the accelerator. The results of preliminary measurements performed in a spare LHC UPS are presented in Appendix D. Further observations and experiments are necessary to identify the exact mechanism that is responsible for the high-frequency cluster.

TABLE III. The summary of the observations for the low and high-frequency cluster.

Low-frequency cluster[a]	High-frequency cluster[b]
Presence of 50 Hz harmonics	
Frequency evolution from the mains	
Phase advance Q7-Q9 compatible with betatronic	
Dipolar nature	
Mainly in the horizontal plane	
Larger amplitudes in Beam 1	
Impact from IP1/5 phase scan	Impact from change of tune
Impact from active filters	Mitigation from transverse damper

[a]Extending up to 3.6 kHz.
[b]Located at 7–8 kHz, depending on the tune.

III. SUMMARY AND CONCLUSIONS

The purpose of the current study was to investigate the origin of the 50 Hz harmonics, an effect that has been observed in the beam signal since the start of the LHC operation. For this reason, a detailed review of the beam spectrum during several beam and machine configurations has been performed that revealed the existence of harmonics in two regimes in the frequency domain: the low-frequency cluster that extends up to 3.6 kHz and the high-frequency cluster at the location $f_{\mathrm{rev}} - f_x$. The methodology presented in this paper allowed us to identify, for the first time in the LHC operation, the existence of the high-frequency cluster on the beam signal. Although many similarities have been identified between the low and high-frequency cluster, the need to distinguish the two regimes is justified by their different response when modifications in the machine configuration are applied.

It is concluded that the two regimes are the result of a real beam excitation. A common signature between the two clusters has been identified; both regimes consist of a set of 50 Hz harmonics, that experience a similar frequency evolution induced by the mains. Based on the fact that the harmonics are multiples of 50 Hz rather than sidebands around the tune, and that the horizontal plane is mainly affected, it is concluded that the nature of the source is dipolar.

In terms of amplitude, an asymmetry between the two clusters has been identified. In particular, more significant amplitudes of the beam oscillations are reported for the high-frequency cluster. During the proton run of 2018, the measured effect of the power supply ripple in the horizontal

plane of Beam 1 was larger than the one of Beam 2 by a factor of two.

As far as the low-frequency cluster is concerned, a correlation with the eight thyristor, line-commutated power supplies of the Main Bends is established, through experiments with the active filters. It is concluded that the eight power supplies of the main dipoles are the source of the low-frequency cluster in the transverse beam spectrum. It is the first time that such a correlation has been demonstrated in the LHC operation.

The amplitude of the beam oscillations in the high-frequency cluster is larger if compared to the low-frequency cluster, hence the importance to identify its origin. If both clusters emerge from a common source, the question that arises is what is the mechanism that allows these high-frequency components to excite the beam. Oscillations at such high frequencies are expected to be significantly attenuated by the shielding effect of the beam screen in the dipole magnets. A review of the power supply's voltage spectrum reveals that there is a reduction of the ripple with increasing frequency.

On the contrary, experimental observations indicate the presence of important spectral components in the high frequency cluster. More interestingly, the amplitude increase of the lines when the ADT settings are modified indicates that, in normal operation, a mitigation of the high-frequency cluster occurs due to the transverse damper. This fact underlines that, in the absence of the damper, the amplitude of the high-frequency cluster is expected to be further enhanced. The exact mechanism responsible for the appearance of the high-frequency cluster on the beam spectrum must be identified in the future operation of the accelerator.

Based on the source and the fact that no modifications are foreseen for the power supplies of the main dipoles, the 50 Hz harmonic are also expected to be present in the HL-LHC era. It has been demonstrated that the transverse damper can effectively reduce the amplitude of these harmonics and its capabilities can be employed in the future to mitigate this power supply ripple perturbation.

The analysis presented in this paper improves our understanding of the ripple effects that were present during the LHC operation. In the context of these studies, a general framework for the analysis of the experimental data has been developed, which can also be used to address other types of noise effects.

ACKNOWLEDGMENTS

The authors gratefully acknowledge H. Bartosik, A. Bland, O. S. Brüning, X. Buffat, J.-P. Burnet, L. R. Carver, R. De Maria, D. Gamba, R. T. Garcia, M. Martino, V. Montabonnet, N. Mounet, D. Nisbet, H. Thiesen, Y. Thurel and J. Wenninger for valuable suggestions and discussions on this work. We would like to thank D. Valuch and M. Soderen for all ADT related measurements and experiments, T. Levens for the MIM measurements and discussions, M. C. Bastos and C. Baccigalupi for the power supply acquisitions and discussions and J. Olexa for the DOROS measurements. Research supported by the HL-LHC project.

APPENDIX A: BEAM SPECTRUM FROM BUNCH-BY-BUNCH ACQUISITIONS

In the presence of a regular filling scheme, the bunch-by-bunch and turn-by-turn ADTObsBox data can be combined to increase the effective bandwidth of the instrument. Signal averaging is not only needed to access the high-frequency components of the signal without aliasing, but also to reduce the noise floor of the spectrum compared to the single bunch case. Averaging the signals of N_b bunches yields a $\sqrt{N_b}$ increase in the signal to noise ratio, in the presence of random noise with zero mean that is uncorrelated with the signal [54].

The spectrum of individual bunches and after averaging over all the bunches in the machine is shown in Fig. 20 for the horizontal plane of Beam 1, for a physics fill and a window length of 4×10^4 turns. The colored lines show the envelope of the spectra of several individual bunches, which is computed by setting a parametric peak threshold of 2×10^{-3} σ. The single bunch noise floor is approximately one order of magnitude higher than the 50 Hz harmonics and thus, signal averaging is necessary.

The time delay Δt_i of a trailing bunch i with respect to the first bunch in the machine, considered as the reference, results in a phase angle:

$$\Delta\phi_i = 2\pi f \Delta t_i, \tag{A1}$$

where f is the frequency under consideration. Consequently, the dephasing of the signals across the ring is proportional to the frequency and the longitudinal spacing of the bunches in the machine.

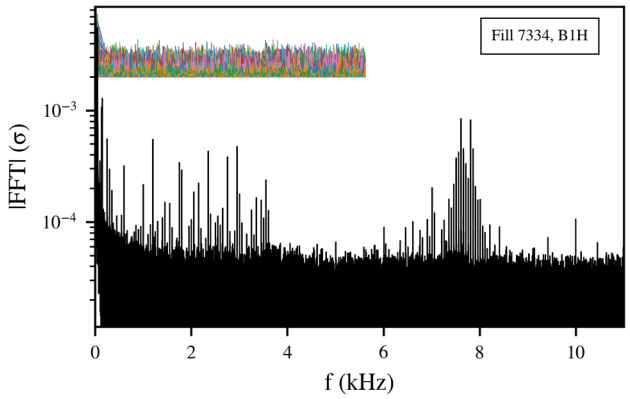

FIG. 20. The spectral envelope of several individual bunches (colored lines) and the spectrum after averaging over all the bunches in the machine (black).

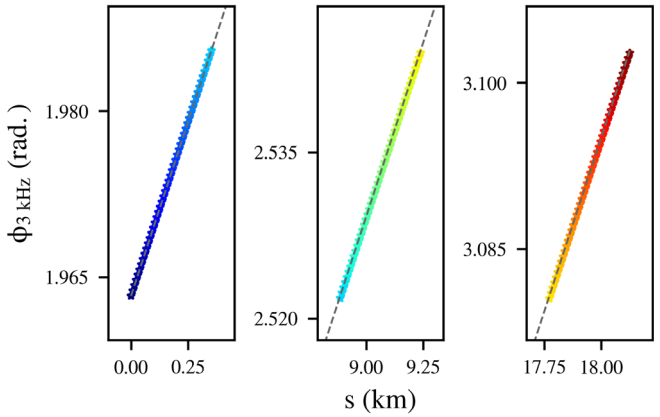

FIG. 21. Phase evolution of the excitation at 3 kHz as a function of the bunch position for three trains of 48 bunches in the LHC ring. The dashed gray line represents the expected dephasing computed from Eq. (A1).

To illustrate this effect, three trains of 48 bunches are considered in simulations with a dipolar excitation at 3 kHz. The bunch spacing is 25 ns and the trains are equally spaced in the LHC ring. The complex spectrum is computed for each bunch and the phase evolution of the 3 kHz line is extracted.

Figure 21 depicts the phase evolution of the excitation for the three trains as a function of the bunch position in the ring. The color code represents the bunch number and the gray line is the expected phase evolution of Eq. (A1), with respect to the first bunch that is considered as the reference. The linear phase evolution of an excitation across the trains in the machine has been experimentally verified by injecting power supply ripple with the transverse damper kicker.

For frequencies much lower than the sampling frequency ($f \ll f_{\mathrm{rev}}$), the dephasing is negligible and the bunch-by-bunch data can be directly averaged in time domain. For frequencies comparable to the revolution frequency, such as the high-frequency cluster, the dephasing between the bunches cannot be neglected. In this case, simply averaging the bunch-by-bunch information will lead to an error in the resulting metric. To illustrate this effect, the first bunches of the three trains are selected.

Figure 22 illustrates the spectra for the first bunches [Fig. 22(a)] of the first (black), second (blue), and third (green) train, respectively, in the presence of a dipolar excitation at 3 kHz. The excitation results in an offset of 13.9 μm (red dashed line), while the second peak corresponds to the betatron tune.

Then, the complex Fourier coefficients at 3 kHz are computed. Figure 22(b) presents the vector of the excitation in the spectrum, whose angle corresponds to the phase of the excitation, for each bunch (left). For a filling scheme consisting of three trains located in azimuthally symmetric locations in the ring, the dephasing at 3 kHz is important. Averaging over the three vectors without correcting for the

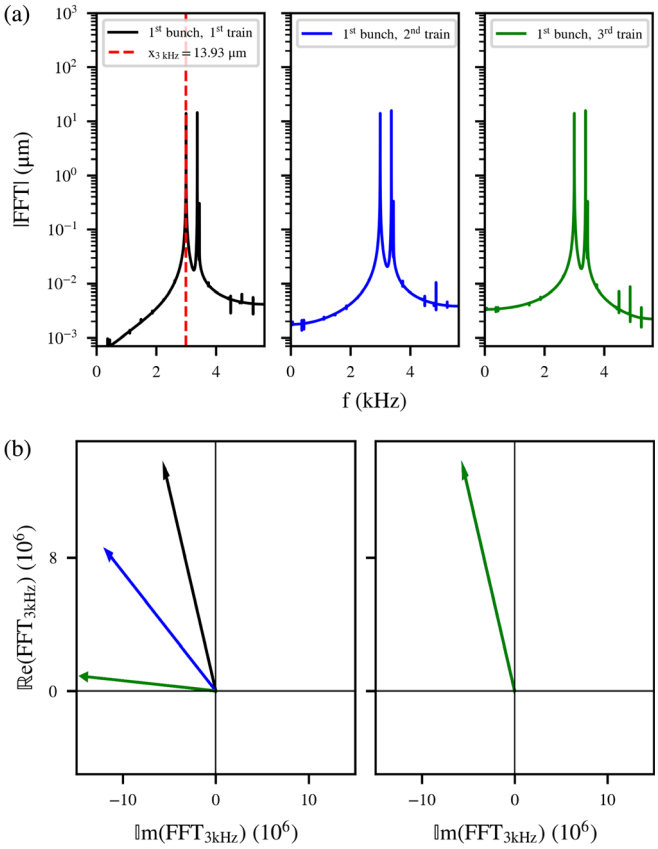

FIG. 22. (a) Spectrum of the first bunches of the first (black), second (blue), and third (green) train in the presence of a dipolar excitation at 3 kHz (red dashed line). (b) Phase of the excitation for the three bunches before (left) and after (right) the correction as computed from Eq. (A2).

dephasing will lead to an error in the offset of the final spectrum.

To this end, an algorithm that applies a phase correction has been implemented. The steps of the method are the following: first, the complex spectra $F_i(\omega)$ are computed for each bunch, where $\omega = 2\pi f$. Then, a rotation is applied to correct for the dephasing of Eq. (A1). The impact of the rotation is depicted in the second plot of Fig. 22(b). Finally, the average over all bunches is computed. The procedure is described by the following expression:

$$F(\omega) = \frac{1}{N_b}\sum_{i=1}^{N_b} F_i(\omega)\mathrm{e}^{-j\omega\Delta t_i}. \tag{A2}$$

APPENDIX B: IMPACT OF THE FREQUENCY EVOLUTION OF THE FUNDAMENTAL FREQUENCY ON ITS HARMONICS

This section presents the impact of a frequency evolution on a harmonic dipolar excitation, similar to the one observed in the 50 Hz harmonics. To simulate this effect,

a single particle is tracked in the LHC lattice using the single-particle tracking code SIXTRACK in the presence of a dipole field error [55,56].

To mimic a non-linear transfer function, similar to the ones of the LHC power supplies, the dipole strength is modulated with the absolute value of a sinusoidal function:

$$\Delta k(t) = |A_r \cos(\omega t)|, \tag{B1}$$

where t is the time, A_r the amplitude and $\omega = 2\pi f_m$ the angular frequency, which experiences a low-frequency evolution. The expression of ω as a function of the fundamental frequency ω_0 is:

$$\omega = \omega_0 + A_{\mathrm{FM}} \sin(\omega_{FM} t), \tag{B2}$$

where A_{FM} is the amplitude and ω_{FM} the frequency of the low-frequency evolution. Using the Fourier trigonometric series expansion of the absolute value of the cosine function:

$$|\cos(\omega t)| = \frac{2}{\pi} + \frac{4}{\pi}\sum_{m=1}^{m=\infty} \frac{(-1)^m}{1-4m^2}\cos(2m\omega t), \tag{B3}$$

and replacing with the time varying angular frequency of Eq. (B2) yields:

$$|\cos(\omega t)| = \frac{2}{\pi} + \frac{4}{\pi}\sum_{m=1}^{m=\infty} \frac{(-1)^m}{1-4m^2} \times \cos(2m\omega_0 t + 2mA_{\mathrm{FM}} \sin(\omega_{\mathrm{FM}} t)t). \tag{B4}$$

The first term within the cosine function of Eq. (B4) reveals that the nonlinear transfer function of Eq. (B1) leads to the excitation of all the even harmonics of the fundamental angular frequency ω_0. Similarly, using a sine function results in the excitation of odd harmonics. The second term describes the low-frequency evolution of these harmonics with a frequency of ω_{FM} and an amplitude equal to $2mA_{\mathrm{FM}}$, which thus, depends on the order of the harmonic.

Figure 23 illustrates the spectrogram as computed from the tracking simulation for a frequency range up to 1.8 kHz, color-coded with the PSD with a fundamental frequency $f_0 = 100$ Hz. All harmonics experience a similar frequency evolution with a peak-to-peak variation proportional to the order of the harmonic as described in Eq. (B4).

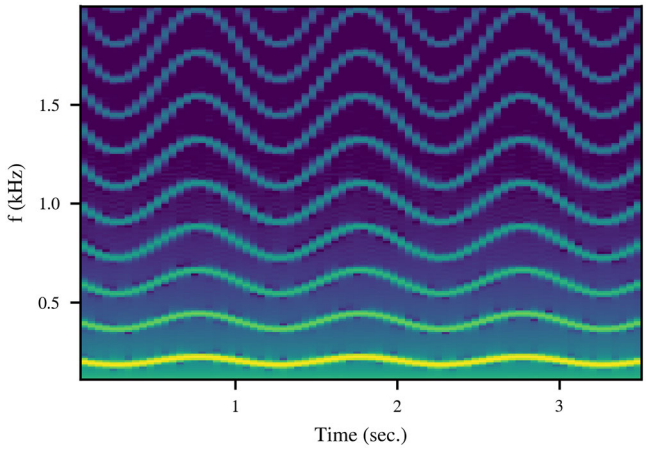

FIG. 23. The impact of a low-frequency excitation on a harmonic dipolar excitation described in Eq. (B1) for a fundamental frequency $f_0 = 100$ Hz.

APPENDIX C: VOLTAGE SPECTRUM OF A SILICON CONTROLLED RECTIFIER

The SCR power supplies of the LHC main dipoles are three-phase full-wave controlled rectifiers. In the following section, a simplified model of a 6 pulse rectifier is used to demonstrate the presence of harmonics in its output voltage. The results can be extended to the 12 pulse LHC main dipole rectifiers using two 6 pulse bridges with a phase shift of 30 degrees. A more detailed model of a SCR power supply and its spectrum can be found in [18].

To obtain an output voltage on the load, two thyristors must simultaneously conduct. Figure 24 presents the output voltage due to the three pairs of conducting thyristors (black, blue and green dashed lines) as a function of the phase. The output voltage as a result of the rectification process (gray line) is also depicted for a firing angle of $\alpha = 0$ (top) and $\alpha = 30$ degrees (bottom).

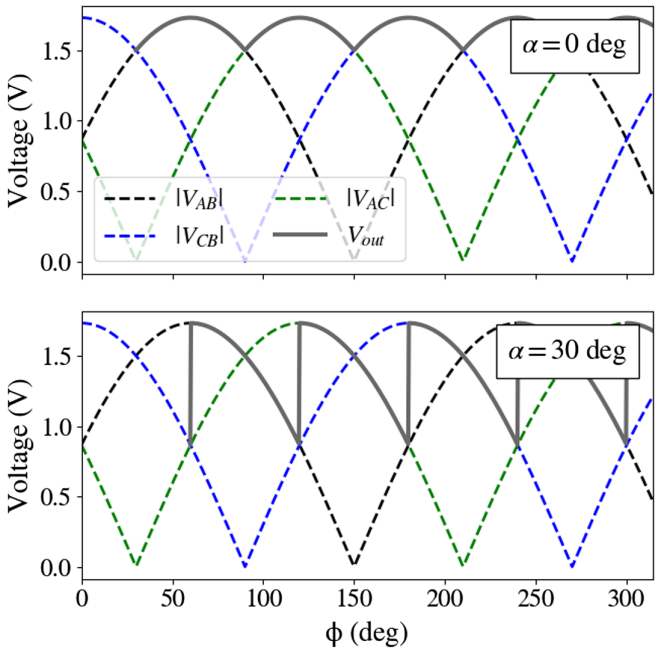

FIG. 24. The output voltage of the three pairs of conducting thyristors (black, blue and green) as a function of the phase. The gray line illustrates the output voltage due to the rectification process for a firing angle of $\alpha = 0$ (top) and $\alpha = 30$ degrees (bottom).

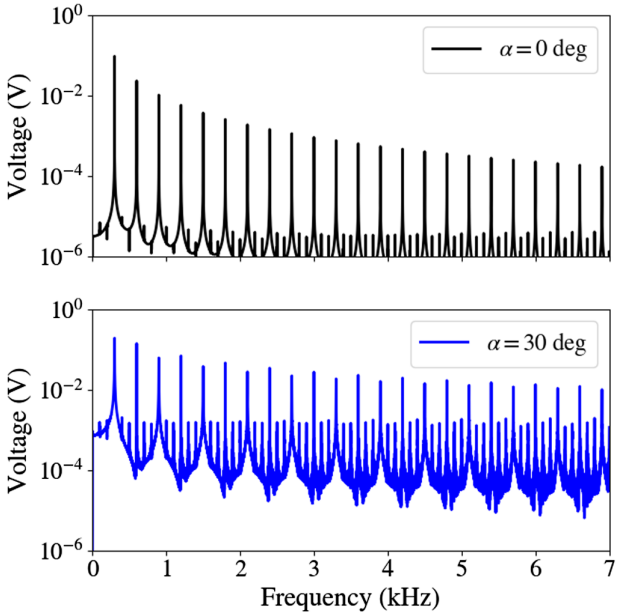

FIG. 25. The frequency spectrum of the SCR rectifier (gray line in Fig. 24) for a firing angle of $\alpha = 0$ (top) and $\alpha = 30$ degrees (bottom).

The Fourier analysis of this signal is shown in Fig. 25 for the two cases. As presented in Appendix B, a non-linear transfer function such as the rectification process results in the appearance of harmonics of the fundamental frequency. For $\alpha = 0$ degrees, harmonics of 300 Hz are present, while several other harmonics of the mains frequency are excited for non-zero values of the firing angle.

APPENDIX D: MEASUREMENTS OF A SPARE LHC UNINTERRUPTIBLE POWER SUPPLY VOLTAGE SPECTRUM

Measurements of the voltage of a spare LHC UPS took place during the second Long Shutdown (LS2) of the accelerator to determine whether the UPS is a potential candidate for the high-frequency cluster observed on the LHC transverse beam spectrum. An oscilloscope was connected to the output of a double-conversion UPS of the same type as the systems present in the accelerator. The configuration of the measured system was similar to the one used during the operation with beam (normal mode operation) [57,58]. In normal mode operation, the AC input is connected to the rectifier and the output DC power is used as an input to the inverter, the output of which feeds the load.

Figure 26 presents the spectrum of the UPS output voltage in normal operation mode (blue) for a frequency range extending up to 12 kHz. For comparison, the noise due to the instrumentation system and other environmental factors was also measured (black). A zoomed window of the spectrum is included (light blue) to illustrate that the

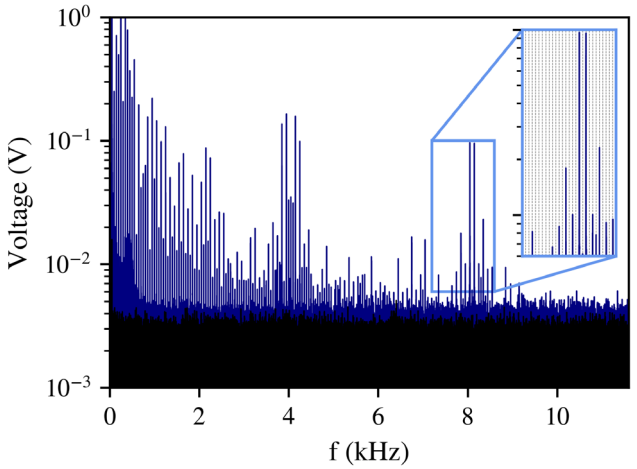

FIG. 26. The UPS output voltage spectrum in normal operation mode (blue) and with a zoomed window (light blue). The vertical gray lines represent the multiples of 50 Hz. The spectrum measured due to environmental noise is also illustrated (black).

distinct spectral components correspond to 50 Hz harmonics (gray lines). In particular, apart from the low-order 50 Hz harmonics, the UPS spectrum contains clusters of 50 Hz harmonics around 4 kHz and 8 kHz. These regimes correspond to the switching frequency of the inverter (4 kHz) and its first harmonic. The existence of 50 Hz harmonics as sidebands around the inverter's switching frequency and its harmonics is an expected feature as the inverter is based on pulse width modulation (PWM) technology [59]. Therefore, the UPS system spectrum contains 50 Hz harmonics in a regime that corresponds to the high-frequency cluster observed on the beam spectrum.

The spectrogram of the UPS output voltage is computed to determine whether the harmonics produced by the UPS system have a similar frequency evolution as the one

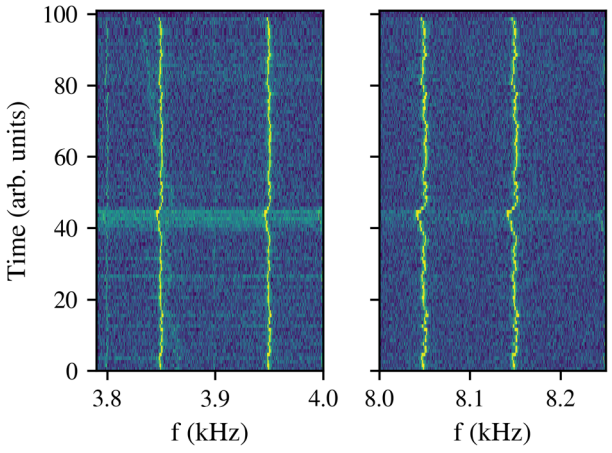

FIG. 27. The UPS spectrogram in normal mode of operation centered around the low-frequency cluster (left) and the high-frequency cluster (right). The color-code represents the PSD.

observed on the harmonics of the beam (see Sec. II B). Figure 27 depicts the spectrogram, color-coded with the PSD and centered around a frequency regime that corresponds to the low-frequency (left) and high-frequency cluster (right) of the beam. These measurements validate that the UPS 50 Hz harmonics experience a frequency evolution with similar characteristics as the one observed on the 50 Hz harmonics of the beam. Based on these observations, the UPS system is a potential candidate for the high-frequency cluster observed on the beam. However, additional measurements are needed with beam during the next operation of the accelerator to investigate whether a correlation of the UPS noise and the high-frequency cluster of the beam can be established.

[1] T. J. Satogata, Nonlinear resonance islands and modulational effects in a proton synchrotron, Ph.D. thesis, Northwestern U., 1993.

[2] F. Zimmermann, Emittance growth and proton beam lifetime in HERA, Ph.D. thesis, Hamburg U., 1993.

[3] O. S. Brüning and F. Willeke, Diffusion-like processes in proton storage rings due to the combined effect of nonlinear fields and modulational effects with more than one frequency, in *European Particle Accelerator Conference (EPAC 1994)* (1994), https://accelconf.web.cern.ch/e94/PDF/EPAC1994_0991.PDF.

[4] O. S. Brüning, M. Seidel, K. Mess, and F. Willeke, Measuring the effect of an external tune modulation on the particle diffusion in the proton storage ring of HERA, Tech. Rep. No. P00021147, 1994.

[5] O. S. Brüning, P. Collier, P. Lebrun, S. Myers, R. Ostojic, J. Poole, and P. Proudlock, LHC Design Report, CERN Yellow Reports: Monographs (CERN, Geneva, 2004).

[6] M. Kuhn, G. Arduini, J. Emery, A. Guerrero, W. Hofle, V. Kain, F. Roncarolo, M. Sapinski, M. Schaumann, and R. Steinhagen, LHC Emittance preservation during the 2012 run., in *Proceedings, 4th Evian Workshop on LHC beam operation: Evian Les Bains, France, December 17-20, 2012* (2012), pp. 161–170, https://cds.cern.ch/record/2302436.

[7] S. C. Cave, R. De Maria, M. Giovannozzi, M. Ludwig, A. MacPherson, S. Redaelli, F. Roncarolo, M. S. Camillocci, and W. V. Delsolaro, Non-linear beam dynamics tests in the LHC: Measurement of intensity decay for probing dynamic aperture at injection, Report No. CERN-ATS-Note-2013-025 MD, 2013, https://cds.cern.ch/record/1543434.

[8] G. Arduini, 50 Hz lines studies: First observations, https://indico.cern.ch/event/436679/contributions/1085928 (2015), accessed: 2019-12-13.

[9] R. De Maria, Observation of 50 Hz lines in the LHC BBQ system, https://lhc-beam-operation-committee.web.cern.ch/lhc-beam-operation-committee (2012), accessed: 2019-12-14.

[10] T. Linnecar and W. Scandale, *Phenomenology and causes of the 50 Hz spaced lines contaminating the Schottky signal*, Tech. Rep. No. CERN-SPS-DI-MST-TL-WS-EEK, CERN-SPS-Improvement-Report-203 (CERN, Geneva, 1986).

[11] X. Altuna *et al.*, The 1991 dynamic aperture experiment at the CERN SPS, AIP Conf. Proc. **255**, 355 (1992), https://aip.scitation.org/doi/pdf/10.1063/1.42289.

[12] O. S. Brüning, Diffusion in a FODO cell due to modulation effects in the presence of nonlinear fields, Part. Accel. **41**, 133 (1992).

[13] W. Fischer and M. Giovannozzi, Dynamic aperture experiment at a synchrotron, Phys. Rev. E **55**, 3507 (1997).

[14] M. Gasior and R. Jones, The principle and first results of betatron tune measurement by direct diode detection, Tech. Rep. No. LHC-Project-Report-853, CERN-LHC-Project-Report-853 (CERN, Geneva, 2005), revised version submitted on 2005-09-16 09:23:15.

[15] O. S. Brüning, M. Seidel, K. Mess, and F. Willeke, Measuring the effect of an external tune modulation on the particle diffusion in the proton storage ring of HERA, Tech. Report No. P00021147, 1994.

[16] O. S. Brüning and F. Willeke, Reduction of particle losses in HERA by generating an additional harmonic tune modulation, in *Proceedings Particle Accelerator Conference*, Vol. 1 (1995), pp. 420–422, https://accelconf.web.cern.ch/p95/ARTICLES/MPG/MPG07.PDF.

[17] P. Cameron, M. Gasior, R. Jones, and C. Tan, The effects and possible origins of mains ripple in the vicinity of the betatron spectrum, Tech. Rep. (Brookhaven National Lab.(BNL), Upton, NY, 2005).

[18] P. Cameron, M. Gasior, R. Jones, and C. Tang, Observations of direct excitation of the betatron spectrum by mains harmonics in RHIC, Tech. Rep. (Brookhaven National Laboratory (BNL) Relativistic Heavy Ion Collider, 2006).

[19] C.-Y. Tan, Novel tune diagnostics for the Tevatron, in *Proceedings of the 2005 Particle Accelerator Conference* (IEEE, New York, 2005), pp. 140–144.

[20] V. Shiltsev, G. Stancari, and A. Valishev, Ambient betatron motion and its excitation by "ghost lines" in Tevatron, J. Instrum. **6**, P08002 (2011).

[21] S. Kostoglou, G. Arduini, L. Intelisano, Y. Papaphilippou, and G. Sterbini, following paper, Impact of the 50 hz harmonics on the beam evolution of the large hadron collider, Phys. Rev. Accel. Beams **24**, 034002 (2021).

[22] M. S. Camillocci, S. Redaelli, R. Tomás, and J. Wenninger, Combined Ramp and Squeeze to 6.5 TeV in the LHC, in *Proceedings, 7th International Particle Accelerator Conference (IPAC 2016): Busan, Korea, May 8-13, 2016* (JACoW, Geneva, 2016), p. TUPMW031.

[23] S. Fartoukh, Achromatic telescopic squeezing scheme and application to the LHC and its luminosity upgrade, Phys. Rev. Accel. Beams **16**, 111002 (2013).

[24] B. Muratori and T. Pieloni, Luminosity levelling techniques for the LHC (2014) pp. 177–181. 5 p, comments: 5 pages, contribution to the ICFA Mini-Workshop on Beam-Beam Effects in Hadron Colliders, CERN, Geneva, Switzerland, 18-22 Mar 2013.

[25] N. Karastathis, K. Fuchsberger, M. Hostettler, Y. Papaphilippou, and D. Pellegrini, Crossing angle anti-leveling at the LHC in 2017, J. Phys. Conf. Ser. **1067**, 022004 (2018).

[26] M. Gasior, Faraday cup award: High sensitivity tune measurement using direct diode detection, Conf. Proc. **C1204151**, MOAP02 (2012).

[27] O. Jones, LHC beam instrumentation, in *2007 IEEE Particle Accelerator Conference (PAC)* (IEEE, New York, 2007), pp. 2630–2634.

[28] L. Carver, X. Buffat, A. Butterworth, W. Höfle, G. Iadarola, G. Kotzian, K. Li, E. Métral, M. O. Sandonís, M. Söderén, and D. Valuch, Usage of the transverse damper observation box for high sampling rate transverse position data in the LHC, in *8th Int. Particle Accelerator Conf. (IPAC'17), Copenhagen, Denmark, May 2017* (JACoW, Geneva, 2017), pp. 389–392; Report No. CERN-ACC-2017-117.

[29] M. Ojeda Sandonís, P. Baudrenghien, A. Butterworth, J. Galindo, W. Höfle, T. Levens, J. Molendijk, F. Vaga, and D. Valuch, Processing high-bandwidth bunch-by-bunch observation data from the RF and transverse damper systems of the LHC, in *Proceedings, 15th International Conference on Accelerator and Large Experimental Physics Control Systems (ICALEPCS 2015): Melbourne, Australia, October 17-23, 2015* (2015), p. WEPGF062, https://inspirehep.net/literature/1481676.

[30] M. Söderén, G. Kotzian, M. O. Sandonís, and D. Valuch, Online bunch by bunch transverse instability detection in LHC, in *Proceedings, 8th International Particle Accelerator Conference (IPAC 2017): Copenhagen, Denmark, May 14-19, 2017* (JACoW, Geneva, 2017), p. MOPAB117.

[31] T. Persson, J. M. C. de Portugal, A. Garcia-Tabares, M. Gąsior, A. Langner, T. Lefèvre, E. Maclean, L. Malina, J. Olexa, P. Skowroński, and R. Tomás, Experience with DOROS BPMs for coupling measurement and correction, in *7th Int. Particle Accelerator Conf.(IPAC'16), Busan, Korea, May 8-13, 2016* (JACOW, Geneva, Switzerland, 2016), pp. 303–305.

[32] J. Olexa, O. Ondracek, Z. Brezovic, and M. Gasior, Prototype system for phase advance measurements of LHC small beam oscillations, Tech. Rep. No. CERN-ATS-2013-038 (CERN, Geneva, 2013).

[33] R. J. Steinhagen, M. J. Boland, and T. G. Lucas, A Multi-band-Instability-Monitor for high-frequency intra-bunch beam diagnostics, Report No. CERN-ACC-2013-0294, 2013, https://cds.cern.ch/record/1637764.

[34] T. Levens, T. Lefèvre, and D. Valuch, Initial results from the LHC Multi-Band Instability Monitor, in *Int. Beam Instrumentation Conf.(IBIC'18), Shanghai, China, 09-13 September 2018* (JACOW Publishing, Geneva, Switzerland, 2019), pp. 314–318.

[35] S. Kostoglou *et al.*, MD4147: 50 Hz harmonics perturbation, Tech. Rep. (CERN, Geneva, 2019).

[36] H. Nyquist, Certain topics in telegraph transmission theory, Trans. Am. Inst. Electr. Eng. **47**, 617 (1928).

[37] Network frequency, https://clients.rte-france.com (2020), accessed: 2020-06-03.

[38] M. Buzio, P. Galbraith, S. Gilardoni, D. Giloteaux, G. Golluccio, C. Petrone, L. Walckiers, and A. Beaumont, Development of upgraded magnetic instrumentation for CERN's real-time reference field measurement systems, Conf. Proc. **C100523**, MOPEB016 (2010).

[39] T. Bohl, Functional specification for upgrade of SPS B-train, CERN, Geneva, Switzerland, Rep. EDMS **1689759** (2016).

[40] A. Huschauer, A. Blas, J. Borburgh, S. Damjanovic, S. Gilardoni, M. Giovannozzi, M. Hourican, K. Kahle, G. Le Godec, O. Michels, G. Sterbini, and C. Hernalsteens, Transverse beam splitting made operational: Key features of the multiturn extraction at the CERN Proton Synchrotron, Phys. Rev. Accel. Beams **20**, 061001 (2017).

[41] H. Thiesen and D. Nisbet, Review of the initial phases of the LHC power converter commissioning, Conf. Proc. **C0806233**, THPP132 (2008).

[42] O. S. Brüning, P. Collier, P. Lebrun, S. Myers, R. Ostojic, J. Poole, and P. Proudlock, LHC Design Report, CERN Yellow Reports: Monographs (CERN, Geneva, 2004) Chap. Power converter system.

[43] S. Kostoglou, H. Bartosik, Y. Papaphilippou, G. Sterbini, and N. Triantafyllou, Tune modulation effects for colliding beams in the High Luminosity Large Hadron Collide, Phys. Rev. Accel. Beams **23**, 121001 (2020).

[44] N. Karastathis, S. Fartoukh, S. Kostoglou, Y. Papaphilippou, M. Pojer, A. Poyet, M. S. Camillocci, and G. Sterbini, MD 3584: Long-Range Beam-Beam 2018, Tech. Rep. (CERN, Geneva, 2020).

[45] A. Verweij, V. Baggiolini, A. Ballarino, B. Bellesia, F. Bordry, A. Cantone, M. Casas Lino, A. Serra, C. Trello, N. C. Lasheras, Z. Charifoulline, G. Coelingh, K. Dahlerup-Petersen, G. D'Angelo, R. Denz, S. Feher, R. Flora, M. Gruwé, V. Kain, and M. Zerlauth, Performance of the main dipole magnet circuits of the LHC during commissioning, *EPAC 2008—Contributions to the Proceedings* (2008).

[46] O. S. Brüning, P. Collier, P. Lebrun, S. Myers, R. Ostojic, J. Poole, and P. Proudlock, Power converter system, in LHC Design Report, CERN Yellow Reports: Monographs (CERN, Geneva, 2004), Chap. 10, pp. 275–307.

[47] J.-P. Burnet, Test results of RPTE LHC thyristor rectifier with active filter (to be published).

[48] G. Apollinari, I. B. Alonso, O. Brüning, P. Fessia, M. Lamont, L. Rossi, and L. Tavian, High-Luminosity Large Hadron Collider (HL-LHC), CERN Yellow Rep. Monogr. **4**, 1 (2017).

[49] F. Dubouchet, W. Hofle, G. Kotzian, and D. Valuch, "What you get"—Transverse damper, in *Proceedings, 4th Evian Workshop on LHC beam operation: Evian Les Bains, France, December 17-20, 2012, CERN* (CERN, Geneva, 2012), pp. 73–78.

[50] J. P. O. Komppula, G. Kotzian, S. Rains, M. Söderén, and D. Valuch, ADT and ObsBox in LHC Run 2, plans for LS2, in *Proceedings, 9th Evian Workshop on LHC beam operation: Evian Les Bains, France, January, 2019* (2019), http://cds.cern.ch/record/2750292.

[51] M. Morrone, M. Martino, R. De Maria, M. Fitterer, and C. Garion, Magnetic frequency response of High-Luminosity Large Hadron Collider beam screens, Phys. Rev. Accel. Beams **22**, 013501 (2019).

[52] F. Ruggiero, Single beam collective effects in the LHC, Collective effects in large hadron colliders. Proceedings, International Workshop, Montreux, Switzerland, October 17-22, , 1994, Part. Accel. **50**, 83 (1995).

[53] V. Chareyre, Assessment of the high frequency noise produced by the UPS systems in the LHC Machine, Tech. Rep. (CERN, Geneva, 2015).

[54] U. Hassan and S. Anwar, Reducing noise by repetition: Introduction to signal averaging, Eur. J. Phys. **31**, 453 (2010).

[55] SixTrack, http://sixtrack.web.cern.ch/SixTrack/ (2019), accessed: 2019-11-26.

[56] R. D. Maria, J. Andersson, V. K. B. Olsen, L. Field, M. Giovannozzi, P. D. Hermes, N. Høimyr, S. Kostoglou, G. Iadarola, E. Mcintosh, A. Mereghetti, J. W. Molson, D. Pellegrini, T. Persson, M. Schwinzerl, E. H. Maclean, K. Sjobak, I. Zacharov, and S. Singh, SixTrack project: Status, runtime environment, and new developments, in *Proceedings, 13th International Computational Accelerator Physics Conference, ICAP2018: Key West, FL, USA, 20-24 October 2018* (2019), p. TUPAF02, https://inspirehep.net/literature/1736172.

[57] V. Chareyre, Electrical distribution for machine protection systems: how to ensure safe powering and high availability?, in *Machine Protection Panel workshop 2013* (CERN, Geneva, 2013).

[58] V. Chareyre, Assessment of the high frequency noise produced by the UPS systems in the LHC machine (2015, to be published).

[59] B. Wu and M. Narimani, PWM current source inverters, in *High-Power Converters and AC Drives* (Wiley-IEEE Press, New York, 2017), pp. 225–256.